

Virtual slit scanning microscopy

Reto Fiolka · Andreas Stemmer · Yury Belyaev

Accepted: 29 August 2007 / Published online: 20 September 2007
© Springer-Verlag 2007

Abstract We present a novel slit scanning confocal microscope with a CCD camera image sensor and a virtual slit aperture for descanning that can be adjusted during post-processing. A very efficient data structure and mathematical criteria for aligning the virtual aperture guarantee the ease of use. We further introduce a method to reduce the anisotropic lateral resolution of slit scanning microscopes. System performance is evaluated against a spinning disk confocal microscope on identical specimens. The virtual slit scanning microscope works as the spinning disk type and outperforms on thick specimens.

Keywords Confocal microscopy · Microscopy · Scanning microscopy

Introduction

Confocal microscopy, originally invented by Marvin Minsky (1988), is a widely accepted technique to produce sharp optical sections with the aid of a pinhole that rejects out-of-focus blur and scattered light.

The most common system of confocal laser scanning microscope (CLSM) scans a single laser spot across the specimen. It employs a photo multiplier tube (PMT) behind

a physical pinhole aperture as a light detector. Due to the point-by-point scanning, such systems are rather slow. Furthermore, the PMT detector has low quantum efficiency.

Another popular confocal system employs a Nipkow-type spinning disk (Graf et al. 2005) that sweeps a pattern of multiple pinholes across the field and uses a CCD camera for detection. Spinning disk microscopes enable much higher frame rates than the CLSM, but they cannot be easily adapted to different imaging conditions, as the pinhole size and separation are fixed.

Using slit apertures rather than pinholes, can yield an increased signal level and enables faster scanning rates, but the resolution of such system is slightly anisotropic (Pawley 1995; Sheppard and Mao 1988).

In programmable array microscopy (PAM), a digital mirror display (DMD) is used to generate arbitrary excitation patterns (Verveer et al. 1997). The same DMD dissects the fluorescent light into two images, formed by the in-focus light and the out-of-focus light. Using special patterns and post-processing, it is possible to increase the signal level and reduce the acquisition time compared to CLSM.

A further concept combining flexibility in the size and arrangement of pinholes with the high quantum efficiency of CCD cameras was introduced with the virtual pinhole microscope (VPM, Rector et al. 2003). Images of multiple point sources are acquired with a CCD camera and the confocal information is extracted digitally in a post-processing step. A similar approach was previously used to correct aberrations in transmission confocal microscopes (Cogswell and O'Byrne 1992; O'Byrne and Cogswell 1992). Drawback of this concept is the limitation of overall frame rate, because for each pattern position the full CCD frame has to be read out.

R. Fiolka · A. Stemmer (✉) · Y. Belyaev
Nanotechnology Group, ETH Zurich,
Tannenstrasse 3, 8092 Zurich, Switzerland
e-mail: astemmer@ethz.ch

Present Address:
Y. Belyaev
Advanced Light Microscopy Facility,
European Molecular Biology Laboratory,
Meyerhofstr. 1, 69117 Heidelberg, Germany

Here we introduce an extension of the virtual pinhole concept for slit scanning microscopes. As scanning is required only in one dimension or in two dimensions to minimize anisotropy in lateral resolution, image acquisition rate can be increased compared to virtual aperture point scanning. Furthermore, we exploit the fact that, with an interline-transfer CCD camera, separate lines can be read out much faster than an entire image.

Materials and methods

Instrument set up

Figure 1 depicts the optical train of our system. A cylindrical lens focuses a collimated laser beam into a line in the field stop plane. A piezo tip/tilt mirror scans this line across the object plane. The line scan unit attaches to the standard epi-illumination port of a Zeiss Axiovert 200M microscope. To evaluate imaging performance on identical specimens, a CSU-10 spinning disk system (VisiTec) is coupled to the left side port of the same microscope. Orca-ER CCD cameras (Hamamatsu Photonics, Japan) are used for each system. A Zeiss plan-apochromatic 100 \times NA 1.4 oil immersion objective is used for all experiments. Tip/tilt mirror, microscope focus, and image acquisition are controlled using a lab view program.

Data acquisition and processing

While scanning the diffraction-limited line across the specimen, a bright-field image of the illuminated line and its pixel-neighborhood is acquired. The system is calibrated such that (1) the region of interest (ROI) on the CCD chip moves synchronously with the scanning line and (2) the scanning line always stays in the center of the ROI. We set

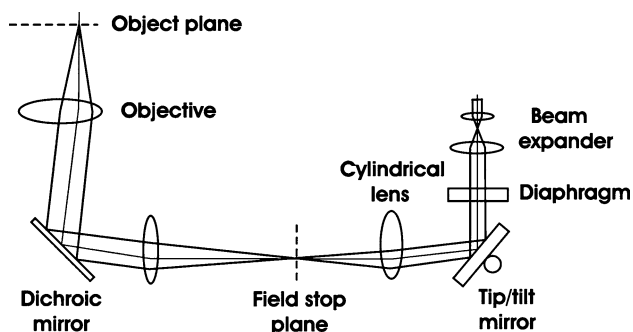


Fig. 1 Optical train of the virtual slit scanning microscope. A laser beam is expanded by a telescope and deflected by a piezo tip/tilt mirror. A cylindrical lens focuses the beam on a line in the field stop plane of the microscope's epi-illumination path. Thereby the line is imaged on the object plane

the width of the ROI to 64 pixels, as this is the minimal size given by the CCD architecture of the camera used. The selective read out of such stripes increases the maximum frame rate of the camera to 60 fps compared to 9 fps for a full image (1,341 \times 1,024 pixels). Hence the minimum acquisition time for a 512 \times 512 pixel image using this camera is 8.5 s. With the advent of more flexible camera architectures, the frame rate could be increased substantially, as the minimal width of the ROI is much larger than that required.

Figure 2 illustrates the acquisition process. At time t_0 , image I_0 of the diffraction-limited line at its initial position is acquired (Fig. 2a). At time t_1 the line has moved by one pixel unit on the specimen and image I_1 is acquired, with the ROI also shifted by one pixel unit on the camera chip (Fig. 2b). Consecutive images are stacked in a three dimensional (3D) x - y - t matrix as shown in the Fig. 2c. Note that the y -axis of this data structure is parallel to the global (specimen) Y -axis shown in Fig. 2a. However, individual images of the stack do not have the same origin, as each one is centered on the corresponding position of the illumination line. Hence, this data structure should not be mistaken for a 3D image stack commonly employed in optical sectioning. The chosen data structure affords straightforward post processing since the confocal image can be read out immediately as an x - t plane. This plane corresponds to an image obtained with a physical aperture with a width of one pixel. Width of the virtual slit aperture

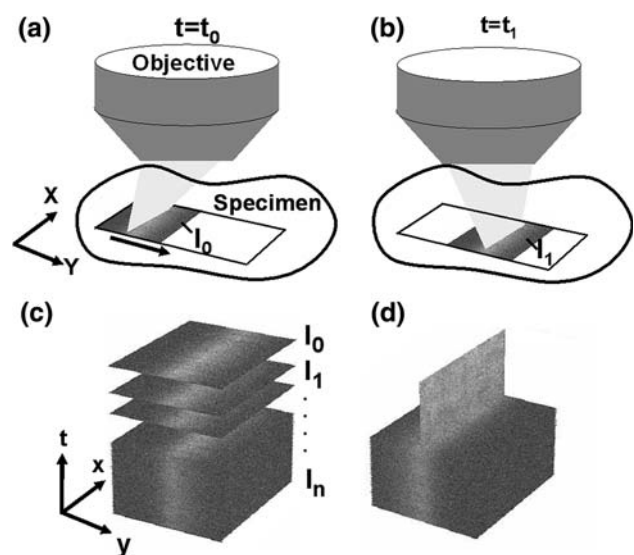


Fig. 2 Schematic illustration of data acquisition and processing: a diffraction-limited line is scanned across the specimen along the Y -direction and for each position an image of the line and its pixel-neighborhood is acquired. **a** at time t_0 , the line is at the initial position and picture I_0 is acquired; **b** at time t_1 , the line has moved by one pixel unit and picture I_1 centered on this new position is acquired; **c** consecutive images (I_0 - I_n) are stored in a three dimensional matrix; **d** the confocal image can be extracted as an x - t plane

can be easily increased by summing adjacent x - t planes to the confocal image plane.

In case the illumination line does not lie parallel to the main axes of the matrix or if the ROI on the CCD chip does not move synchronously with the scanning line, affine transformations (rotation and shear) are applied to correct the alignment.

The simplest way to find the confocal position in the x - y - t matrix is to project (sum up) an individual line image, i.e. x - y plane, along the x -direction (normal to the scan direction) and then finding the position of the maximum in this data. This procedure requires that the particular line image contains an in-focus object. The ratio of peak-intensity to mean-intensity in the data provides a sensitive measure for the presence of an in-focus object. If this ratio is below a certain threshold (we use a threshold of two), it is advised to skip this line image and test the adjacent one.

Bright objects lying close to the line may shift the maximum intensity position from the true line position. Therefore, the line position has to be averaged over several line images.

Alternatively, we propose a global criterion for aligning the virtual aperture. Based on the fact that, for a perfectly aligned confocal aperture, the intensity of objects in the final image is maximized. We assume that with an ideally positioned virtual aperture, the summed intensity of the entire image is maximized. The corresponding algorithm is simple. In each x - t plane, the sum of all pixels is calculated to select the plane having the highest sum. This can also be viewed as a procedure of averaging the maximum intensity position over all the images (I_0 - I_n). Consequently, a possible bias of bright objects lying beside the true line position will be averaged out.

Sample preparation

HeLa cells stably transfected with actin-GFP, were grown on cover slips, fixed, and mounted using Immo-Mount (Shandon, PA, USA). Fluorescent microspheres of 100 and 200 nm diameter (Polyscience Inc. Warrington, PA, USA) were mixed 1:1,000 with 1% Agarose (Sigma-Aldrich, Saint Louis, Missouri, USA) and small drops of this mixture were sandwiched between a glass slide and the cover slip.

Results

Comparing virtual slit scanning with spinning disk microscopy

Figure 3 presents a comparison of 100 nm diameter fluorescent latex microspheres and corresponding averaged

lateral point spread functions (PSF), obtained by virtual slit scanning (Fig. 3a, c) and spinning disk microscopy (Fig. 3b, d). With the virtual slit aperture set smaller than the diameter of the airy disk (192 nm compared to 231 nm), the PSF is sharpened in the scan direction. The full width at half maximum (FWHM) of the PSF measures 211 nm in scan direction and 255 nm along the line. The spinning disk confocal microscope yields an isotropic PSF of 230 nm FWHM.

Figure 4 compares 3D PSFs obtained from the same microspheres. Fig. 4a shows a Y - Z plane and Fig. 4b an X - Z plane of the PSF acquired with the virtual slit scanning microscope. Clearly, the PSF is narrower in the scan direction. In Fig. 4c an X - Z plane of the PSF obtained with the spinning disk confocal microscope is shown. In Z -direction, the FWHM of the PSF amounts to 832 nm for the slit scanning microscope and 823 nm for the spinning disk microscope.

Furthermore, it is striking that Fig. 4a, b contain less noise than Fig. 4c. We assume that the noise in Fig. 4c originates from cross talk between the pinholes of the spinning disk.

Figure 5 demonstrates one of the unique post-processing options of the virtual slit scanning microscope on a data set of a HeLa cell. The width of the virtual aperture and thereby the thickness of the confocal optical section can be set after the image acquisition.

A several micrometer thick slice of an autofluorescent *Convallaria* pollen grain is used to evaluate performance on thick fluorescent specimens (Fig. 6a, b). The image obtained with the virtual slit scanning microscope (Fig. 6a) contains less out-of-focus contributions than the spinning disk image (Fig. 6b). We believe that for thick specimens the separation of pinholes in the spinning disk is not sufficient to avoid cross talk while the virtual slit can efficiently cut off the out-of-focus and the scattered light. Indeed, while imaging the *Convallaria* specimen by virtual slit scanning, large specimen areas adjacent to the excitation line emit light.

In Fig. 6c, d images of the actin-cytoskeleton of a HeLa cell are shown in which parts of the cells are slightly out-of-focus. These two images look similar, but the image obtained with the virtual slit aperture contains more out-of-focus contributions. We interpret these artifacts as a general problem of slit scanners. The slit aperture cannot reject out-of-focus information along the scanning line, and therefore, the optical sectioning power is slightly reduced.

To test whether the out-of-focus information in Fig. 6c could originate from possible misalignment of the virtual slit, we analyzed its position as selected by the global alignment algorithm in data stacks of different specimens. Only for planes with objects completely out-of-focus, we observed deviations in alignment by one pixel.

Fig. 3 Images of 100 nm diameter fluorescent latex microspheres: **a** virtual slit scanning microscope; **b** spinning disk; **c** profiles of the lateral point spread function of the virtual slit scanning microscope plotted in *X*- and *Y*-directions and averaged over ten in-focus beads. The image was scanned in *Y*-direction, **d** profiles of the lateral point spread function of the spinning disk microscope plotted in *X*- and *Y*-directions

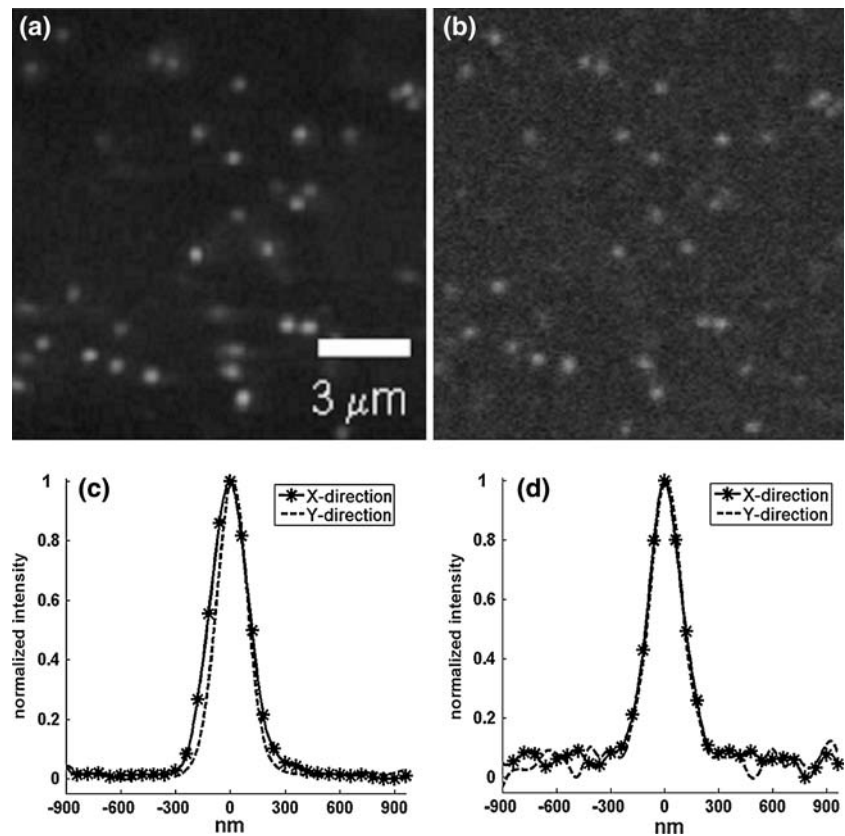


Fig. 4 Comparison of the point spread functions (PSF) of 100 nm diameter fluorescent latex microspheres: **a** *Y*–*Z* PSF of the virtual slit scanning microscope, **b** *X*–*Z* PSF of the virtual slit scanning microscope and a corresponding line profile. The image was scanned in the *Y*-direction, **c** *X*–*Z* PSF of the spinning disk microscope and a corresponding line profile

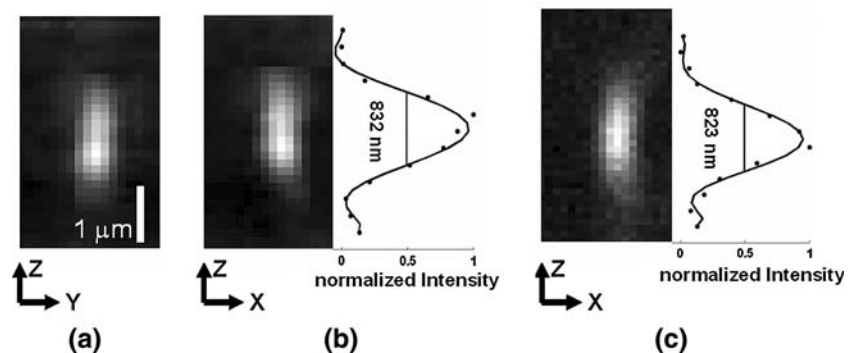


Figure 7 documents accuracy and robustness of our global alignment criterion for different types of specimen, a thin fluorescent layer, HeLa cells, and a fluorescent microsphere sample. Summed intensities of *x*–*t* planes versus the *y*-axis of the data stack are plotted. The global intensity maximum corresponds to the position of the scanning line. Figure 7a nicely demonstrates that, irrespective of the type of specimen (a featureless fluorescent layer or different HeLa cells), the global maximum is at the same position. Figure 7b displays corresponding data for a 3D latex microsphere sample imaged at different focal positions. Again, all global maxima overlap and occur at the same position as in Fig. 7a. Interestingly, the peak of the HeLa cell data sets is sharper than the one corresponding to the microsphere sample, although the HeLa

cells feature a more complicated 3D structure and individual images contain more out-of-focus contributions. We conclude that the global alignment criterion is a powerful and robust tool to determine the exact position of the scanning line and therefore, the confocal image, even in the presence of out-of-focus objects.

Anisotropy reduction in slit scanning

All slit scanning confocal microscopes exhibit anisotropy in lateral resolution, the PSF is sharpened in the scan direction only and out-of-focus contributions are transmitted along the illumination line. Here, we propose a simple method to obtain nearly isotropic lateral resolution

Fig. 5 Variation in the width of the virtual aperture in a data set of an actin-GFP HeLa cell: **a** 64 nm, **b** 448 nm, **c** 832 nm, **d** 1,216 nm

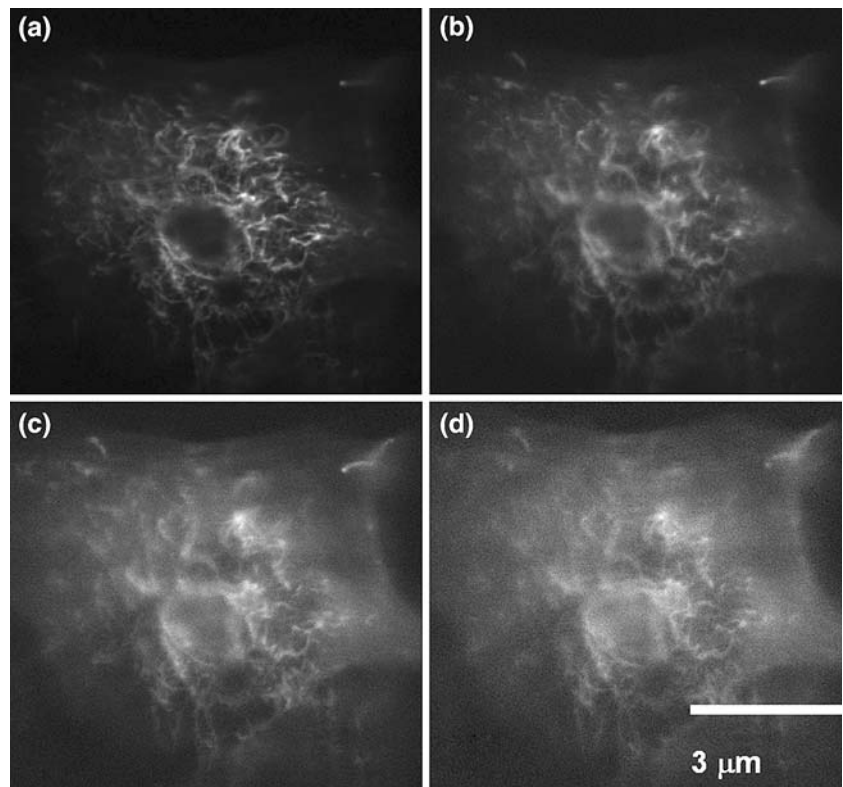
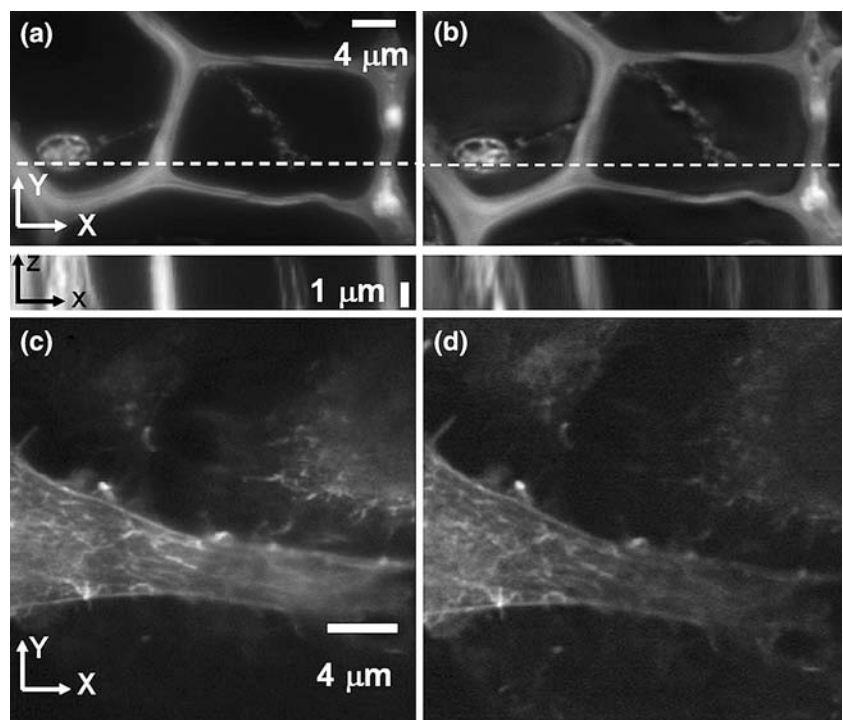


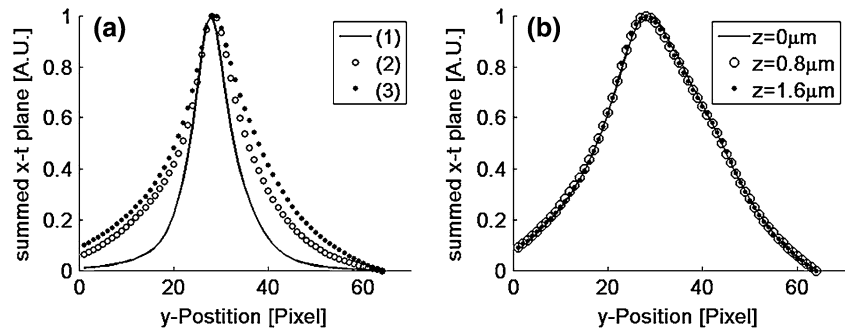
Fig. 6 **a** *X*–*Y* and *X*–*Z* views of a *Convallaria* pollen grain imaged with the virtual slit scanning microscope. The scan direction is in the *Y*-direction, **b** *X*–*Y* and *X*–*Z* views of a *Convallaria* specimen imaged with the spinning disk microscope, **c** *X*–*Y* view of the actin–cytoskeleton of a HeLa cell imaged with the virtual slit scanning microscope, **d** *X*–*Y* view of the HeLa specimen imaged with the spinning disk microscope



with slit scanning microscopes: (1) The object is scanned twice, with the second scan orthogonal to the first one, (2) The Fourier spectra of the two intensity-normalized confocal images are combined such that on the scan axes (i.e. on the corresponding reciprocal axes), only the high-

resolution information is considered, (3) At the origin, the two Fourier spectra are averaged, and (4) The remaining spectrum is a linear combination of both Fourier spectra with azimuthally varying weights. We set the weighting mask for the dataset scanned in *X*-direction to

Fig. 7 Summed x - t plane intensities versus y position for different specimens: **a** thin fluorescent layer *I* and two different HeLa cells 2,3; **b** 100 nm fluorescent latex microspheres imaged at different focal positions



$w_x = \cos^2(\varphi)$ and the mask for the dataset scanned in Y -direction to $w_y = \sin^2(\varphi)$, $\varphi = \arctan(Y/X)$ being the polar angle.

In Fig. 8a and b, two orthogonally scanned images of a group of 200 nm diameter microspheres are shown together with the applied weighting masks for their Fourier spectra. Pairs of closely spaced microspheres can only be resolved in the scanning direction. In the back transformed image (Fig. 8c) of the merged Fourier spectra, pairs of microspheres are clearly resolved in both scanning directions.

This method of anisotropy correction requires two scans and thus increases photobleaching and phototoxicity effects, yet it is still faster than point scanning.

Discussion

A novel set up for virtual slit scanning microscopy has been presented and its optical performance is shown to be comparable with a Nipkow spinning disk microscope. Notwithstanding the reduced sectioning power associated with slit scanning confocal microscopes, the virtual slit scanning microscope yields image quality comparable with a spinning disk microscope. Furthermore, images of thick specimens obtained by virtual slit scanning contain significantly less noise than images acquired with the spinning disk.

An efficient data structure facilitates image reconstruction and robust criteria for optimal alignment of the virtual aperture ensure good performance. Nearly isotropic resolution is achieved using two exposures in orthogonal slit scan directions.

The virtual slit scanning microscope combines the flexibility of a CLSM with the high quantum efficiency of CCD cameras. Furthermore, it offers a unique post-processing option, namely, the variation of the slit width. This feature enables the user to find an optimum between signal level and confocality (ranging from a confocal to a nearly epifluorescent image) after data acquisition. Additionally, the robust automatic numerical alignment of the aperture makes the system very user-friendly. Our concept of virtual aperture is not restricted to slit scanning, but could also be applied to conventional confocal microscopes that do not require a moving aperture as the emission light passes the scanning mirror.

At the moment, the frame rate of our system is low, but it could be easily increased by further reducing the width of the ROI and using fast EM-CCD cameras or by simultaneously projecting multiple parallel lines on the object. Alternatively, a slit scanning microscope could be equipped with a CCD detector containing e.g. five lines. Thereby, it should be feasible to combine all the advantages of the virtual aperture with fast read out capabilities, as each line can have its own amplifier and A/D unit.

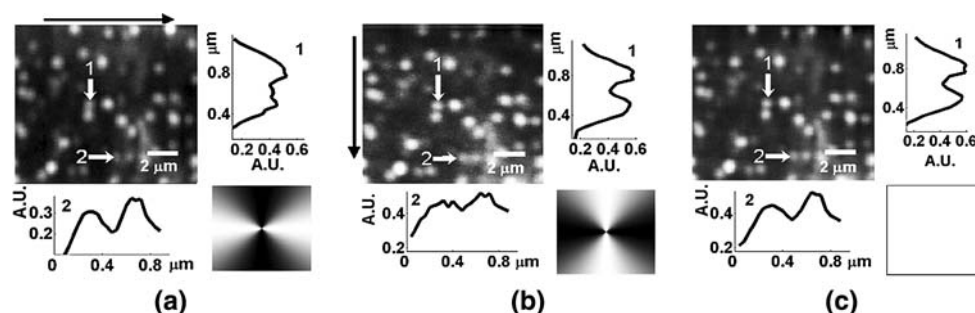


Fig. 8 Line scan induced anisotropy in lateral resolution and its correction demonstrated for a group of 200 nm diameter microspheres *black arrows in a and b indicate the scan direction white arrows point*

to pairs of microspheres and the corresponding profile plots bottom right inserts in a and b are the weighting masks applied to the corresponding spectra; c image computed from the merged spectra

We are confident that the new post-processing options offered by virtual slit scanning microscopy will prove to be very useful in biological and biomedical applications.

Acknowledgments We thank Dr. Andreas Vonderheit for preparing the biological specimens and Dr. Gabor Csúcs of the Light Microscopy Center (LMC) of ETH Zurich for assisting us with the spinning disk confocal microscope.

Reference

- Cogswell CJ, O'Byrne JW (1992) A high resolution confocal transmission microscope: I. System design. In: Acharya RS, Cogswell CJ, Goldgof DB (eds) Biomedical image processing and three-dimensional microscopy. SPIE, Bellingham, pp 503–511
- Graf R, Rietdorf J, Zimmermann T (2005) Live cell spinning disk microscopy. *Microsc Tech* 95:57–75
- Minsky M (1988) Memoir on inventing the confocal scanning microscope. *Scanning* 10(4):128–138
- O'Byrne JW, Cogswell CJ (1992) A high resolution confocal transmission microscope: II. Determining image position and correcting aberrations. In: Acharya RS, Cogswell CJ, Goldgof DB (eds) Biomedical image processing and three-dimensional microscopy. SPIE, Bellingham, pp 512–520
- Pawley JB (1995). Handbook of biological confocal microscopy. Plenum, New York
- Rector DM, Ranken DM, George JS (2003) High-performance confocal system for microscopic or endoscopic applications. *Methods* 30(1):16–27
- Sheppard CJR, Mao XQ (1988) Confocal Microscopes with Slit Apertures. *J Mod Opt* 35(7):1169–1185
- Verveer PJ, Hanley QS, Verbeek PW, Van Vliet LJ, Jovin TM (1997) Theory of confocal fluorescence imaging in the programmable array microscope (PAM). *J Microsc Oxf* 189:192–198